

GazeXPET: An Expert Eye-tracking Dataset for Interpretable and Explainable AI in Oncologic FDG-PET/CT Scans

Joy T Wu^{1,†,*}, Daniel Beckmann^{2,†}, Sarah Miller¹, Alexander Lee¹, Elizabeth Theng¹, Stephan Altmayer¹, Ken Chang¹, David Kersting^{1,5}, Tomoaki Otani^{1,6}, Brittany Z Dashevsky¹, Hye Lim Park^{1,7}, Matteo Novello¹, Kip Guja¹, Curtis Langlotz¹, Ismini Lourentzou⁴, Daniel Gruhl³, Benjamin Risse^{2,††}, and Guido A Davidzon^{1,††}

[†]These first co-authors contributed equally to this work

^{††}These co-senior-authors contributed equally to this work

Affiliations:

¹Division of Nuclear Medicine, Department of Radiology, Stanford University/Stanford Health Care, Stanford, CA 94305, USA.

²University of Münster, Computer Vision and Machine Learning Systems, Heisenbergstraße2, Münster 48149, Germany.

³Google, AI Infrastructure, Mountain View, CA 94043, USA

⁴University of Illinois Urbana-Champaign, School of Information Sciences, Champaign, IL 61820, USA.

⁵Department of Nuclear Medicine, Essen University Hospital, West German Cancer Center, University of Duisburg-Essen, Germany.

⁶Department of Diagnostic Imaging and Nuclear Medicine, Kyoto University, Japan.

⁷Division of Nuclear Medicine, Department of Radiology, Eunpyeong St. Mary's Hospital, College of Medicine, The Catholic University of Korea, Seoul, Korea.

***Corresponding author:** Joy T. Wu (joytyw@stanford.edu)

ABSTRACT

Background:

[18F]FDG-PET/CT is a cornerstone imaging modality for tumor staging and treatment response assessment across many cancer types, yet expert reader shortages necessitate more efficient diagnostic aids. While standalone AI models for automatic lesion segmentation exist, clinical translation remains hindered by concerns about interpretability, explainability, reliability, and workflow integration.

Methods:

We constructed GazeXPErT, a 4D eye-tracking dataset capturing expert search patterns during tumor detection and measurement on 346 FDG-PET/CT scans. Each study was read by a trainee and a board-certified nuclear medicine or radiology specialist using an eye-tracking-enabled annotation platform that simulates routine clinical reads. From 3,948 minutes of raw 60Hz eye-tracking data, 9,030 unique gaze-to-lesion trajectories were extracted, synchronized with PET/CT image slices, and rendered in COCO-style format for multiple machine learning applications. Validation experiments used a 3D nnUNet segmentation model and a vision transformer to assess expert search patterns for lesion segmentation, localization, and intention prediction.

Results:

The 3D nnUNet tumor segmentation model achieved superior performance when incorporating expert gaze patterns versus without (DICE score 0.6819 versus 0.6008). The vision transformer trained on sequential gaze and PET/CT images demonstrated promising baseline improvement in lesion localization (74.95% predicted gaze point closer to tumor) and expert intention prediction (Accuracy 67.53% and AUROC 0.747).

Conclusions:

GazeXPErT captures experts' natural visual reasoning patterns while searching for suspicious malignant lesions in FDG-PET/CTs, providing a valuable resource to facilitate interpretable and explainable AI development and human-AI interaction research. Validation experiments integrating expert gaze into AI training pipelines show promising performance gains, supporting human-in-the-loop approaches to AI in oncologic imaging.

Background

¹⁸F-fluorodeoxyglucose Positron Emission Tomography/Computed Tomography (FDG-PET/CT) offers sensitive identification of metabolically active tumors and has become a clinically crucial volumetric imaging modality for cancer staging and treatment response monitoring¹⁻¹². The PET imaging component uses a radioactively labeled glucose analog to image cells with higher metabolic activities, while CT images provide the corresponding anatomical details to increase diagnostic specificity¹³. Reproducible measurement of index and total tumor burden is important for prognosis^{14, 15}, but is time consuming to do manually. To accurately interpret tumor burden, human experts employ extensive prior knowledge, including anatomy-specific search patterns and cancer-specific metastatic pathways, to differentiate tumors from normal physiological FDG uptake, post-treatment changes, or other alternative diagnoses. These skills are taught interactively between experts of varying experience and individually refined over years of training. The multi-factorial reasoning steps developed allow human experts to read with increased confidence even when encountering cases very different from prior experiences. Crucially, human experts also learn to express appropriate uncertainty when available information is insufficient or inconsistent with the overall clinical picture.

In contrast, current state-of-the-art deep learning models trained to segment or detect tumors in FDG-PET/CT scans are static, initially developed on fixed and often small datasets, and trained without experts' visual reasoning insight¹⁶⁻¹⁹. Although there are techniques to train more robust models through better representation of intrinsic imaging features using self-supervision, attention mechanisms, ensemble models, or contextual multi-modal and multi-tasking models^{20, 21}, they remain standalone AI models that vary in performance and struggle with real life out-of-distribution data. These barriers, along with concern for model bias, interpretability, and explainability, render most research models inadequate for clinical adoption^{22, 23}. Moreover, efficient solutions to integrate automatic AI output into the workflow of imaging specialists, without introducing additional cognitive burden, is still very much an ongoing research problem²⁴⁻²⁶.

Our dataset, GazeXPErT, aims to help address these problems by simultaneously capturing radiology experts' visual reasoning patterns and their task intentions. Human eye movements are task specific and are controlled by the fastest muscles in the body^{27, 28}. Despite vision being the main sensory modality radiologists routinely use to interact with data, there has been limited utilization of gaze in assisting human-AI interactions in radiology workflows. Historically, the majority of eye-tracking research in radiology has focused on exploratory analyses of gaze pattern differences, e.g., stratified along performance lines based on experience or fatigue^{29, 30}. However, there have been growing interests to integrate

eye-tracking with machine learning to develop more trusted and explainable AI models in both the medical and non-medical domains. For example, by mimicking human visual attention^{31–36} and broadening our understanding of the cognitive processes for complex tasks^{37–39}. Overall, there is a growing body of research in radiology utilizing eye-tracking data to train more interpretable models^{40, 41}. Notable examples include: training chest X-rays diagnostic or reporting models with radiologists' search patterns^{32, 42–46}, gaze assisted lesion or anatomy segmentation for CT brain and body^{47–49}, and radiologists scan path prediction for chest X-rays and CT abdomen⁵⁰.

GazeXPERt is a multimodal 4D eye-tracking dataset that captures 13 independent human experts' search patterns while detecting tumors in 346 whole-body FDG-PET/CTs from a public dataset¹⁹. GazeXPERt contributes 9,030 unique gaze-to lesion trajectories derived from 3,948 minutes of raw eye-tracking data (60Hz), rendered in a COCO-style format for machine learning tasks⁵¹. Furthermore, all imaging visualization parameters were recorded simultaneously to enable reconstruction of the entire FDG-PET/CT read. GazeXPERt is designed to explore multiple machine learning problems, including and not limited to, visual grounding or causal reasoning, clinically explainable feature augmentation, human-computer interaction, human intention prediction/understanding, and expert gaze-rewarded modeling. The dataset will be open-sourced via multiple venues, including the Stanford Center for Artificial Intelligence in Medicine and Imaging (AIMI Center) and Kaggle.

This paper details our dataset collection protocol and data schema. We show baseline validation experiments, demonstrating the benefits of training AI models with expert insight and the technical feasibility of training models to predict task-specific expert intentions through their gaze for FDG-PET/CT. Our goal is to motivate clinical and machine learning communities to reimagine diagnostic medical imaging workflows, where human experts and AI can more adaptively leverage each other's insight in real time.

Methods

Data Collection Protocol

A custom eye-tracking PET/CT platform (Figure 1) was built with Python packages to record the search patterns and lesion annotations of human experts while reading FDG-PET/CT studies. 346 unique studies (98 lymphoma, 122 lung cancer, and 126 melanoma) from 343 patients were randomly sampled from an open-source whole-body FDG-PET/CT dataset¹⁹. Each study was re-interpreted by one trainee (five radiology residents and one nuclear medicine fellow) and one experienced board-certified specialist in nuclear medicine and/or diagnostic radiology. The experienced readers come from 4 institutions, including in the United States, Germany, Korea and Japan, providing geographically and institutionally diverse gaze training data. Given the patient's age, gender, and cancer diagnosis, the observer's task was to identify, "gaze-select" and confirm all metabolically active lesions, as well as indicate how likely each lesion was related to cancer ("certain" versus "uncertain"). After a one-on-one eye-tracking platform coaching session, every observer reads the same "inter_observer" practice study at least once before beginning formal data collection. In addition, before each reading session, the readers re-calibrate their gaze to the eye-tracking station's set up using the manufacturer's desktop calibration software.

Readers were instructed to simulate a comprehensive clinical interpretation consistent with routine oncologic PET/CT practice, prioritizing identification of metabolically active lesions relevant to disease staging and overall tumor burden assessment rather than a single predefined clinical endpoint. The inclusion of a "certain" versus "uncertain" lesion label reflects routine clinical PET interpretation, where many FDG-avid findings—particularly small lymph nodes or mildly hypermetabolic foci—cannot be definitely classified without follow-up imaging or additional clinical information. Rather than representing annotation noise, this uncertainty encodes expert diagnostic judgment and confidence, which is a critical but often unmodeled component of real-world oncologic image interpretation. Capturing this uncertainty enables future machine learning models to learn not only where experts look, but how confidently they interpret findings.

Simulated routine clinical PET/CT read set up: A screen-based research eye-tracking device (Tobii Pro Spark⁵²) was used to track a reader's eye movement and pupil sizes, recording corresponding 2D gaze locations on a diagnostic 27-inch screen at a sampling frequency of 60 Hz. Participants were allowed to adjust image contrast and windowing, scroll back and forth between 2D axial image slices (i.e., reasoning through the 3D volume), and switch between three different modalities (PET, CT, fused PET/CT) to identify and confirm malignant lesions. For the PET modality, readers had the additional option to view the

volumetric data in a rotatable upright whole-body Maximum Intensity Projection (MIP) from 12 angles. All image visualization parameters were recorded at 60Hz simultaneously with the corresponding gaze coordinates to allow video-like reconstruction of the entire read process. The original 512×512 CT images and the upsampled (to 512×512) and standardized PET images (i.e., SUV) were read for the study. More detailed annotation protocol can be found on our GitHub repository. **Supplemental Appendix 1 details our data collection protocol.**

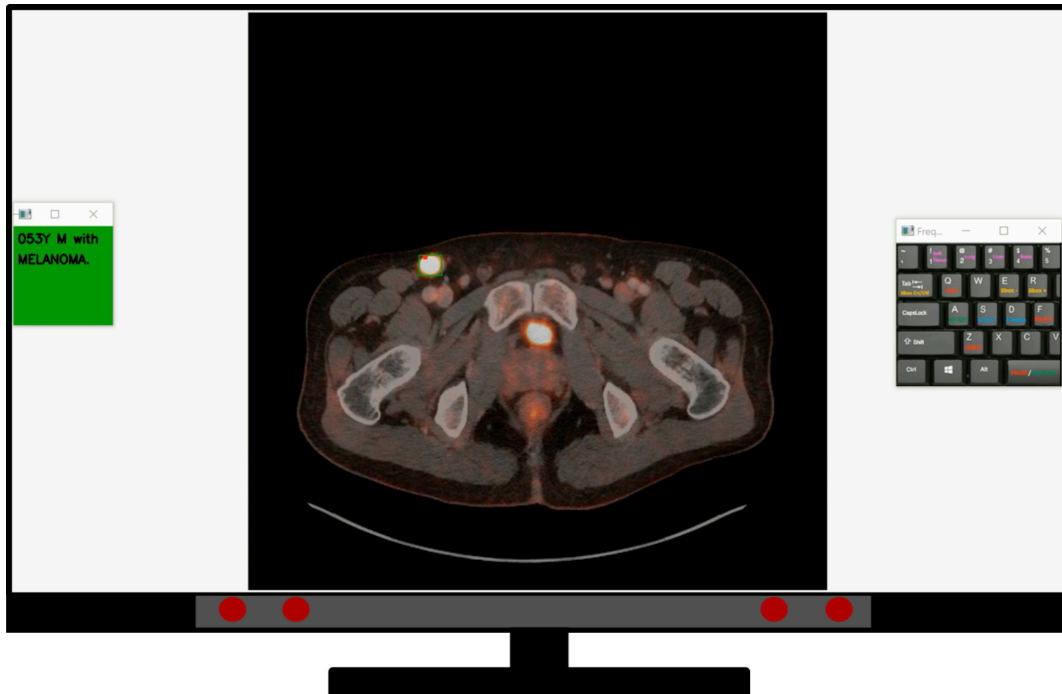


Figure 1. Data collection platform. The PET/CT study was shown to readers in a full-screen application alongside patient age, sex and cancer diagnosis, and a hotkey reminder legend.

Gaze-Assisted Lesion Annotation

Beyond gaze coordinates, ground truth annotations for tumors were collected at the bounding box level at each image slice. The annotation was accelerated semi-automatically via a candidate proposal and validation process, where readers utilized hotkeys to indicate when they wanted to select, accept, reject, or resize a proposed tumor candidate. The proposed bounding box for a lesion could be resized by changing the PET intensity threshold used to generate the candidate via two hotkeys. This PET threshold was recorded and can be used to derive a pseudo-pixel segmentation mask that best estimates the lesion boundary. Notably, readers were instructed to do their best to visually match the PET lesion boundary with the CT lesion boundary when possible. To achieve true recall for the dataset, a baseline candidate lesion proposal algorithm (see details below) was chosen for its high sensitivity so that readers could select almost any suspicious hypermetabolic lesion and not be limited by the misses from an existing AI segmentation model.

Candidate Lesion Proposal Algorithm

The lesion candidate proposal algorithm operates as follows: the last gaze location upon the "select" keystroke is used as the reference point. A user-adjustable maximal SUV (normalized PET) threshold of a slice is used to create pseudo-masks via maximal intensity thresholding, and boxes around masks are calculated via 2D connected components analysis with 8 connectivity. Previously rejected and accepted boxes are filtered out, and the box nearest to the last gaze location is proposed and overlaid over the image slice for display. The size of the box can be adjusted in real-time by increasing or decreasing the SUV segmentation threshold, and the box gets accepted or rejected (for example, because a wrong box is proposed due to inaccurate last gaze point). All key presses are timestamped and saved to discretely record a reader's interactive decisions throughout a study read.

Bounding Box Propagation and Annotation Efficiency

To save time and effort, an accepted box on a "root" (current) slice gets propagated into neighboring slices. Neighboring slices in both z-directions are processed using the saved SUV threshold from the root "accepted" slice. The reader can additionally correct the sizes of the boxes on the adjacent slices separately. The efficiency of this approach is reflected in the annotation time metrics: over 49 hours of gaze data were collected, with a median annotation time per study of 191 seconds and a mean of 259 seconds. The median annotation time per 3D lesion was 0.81 seconds, with a mean of 1.51 seconds. This demonstrates the practical feasibility of our gaze-assisted annotation approach for similar large-scale dataset collection.

Results

GazeXPET dataset collected 3,948 minutes of raw 60Hz expert eye-tracking data with 3D lesion level annotations. **Supplemental Appendix 2 details gaze data quality analysis.** Data Records in **Supplemental Appendix 3 details the postprocessing** done to extract 9,030 unique gaze-to-lesion trajectories, synchronized with the associated PET/CT image slices at 60Hz, and rendered in COCO-style format, friendly for multiple machine learning applications. Here, we show three modeling validation experiments with the GazeXPET dataset for use-case demonstration.

Experiment 1: Value of expert attention for AI tumor segmentation models.

We compared the performance of a standard 3D nnUNet segmentation model trained with and without incorporating gaze heatmap attentional information.

Method: The recommended nnUNet ResEncL-Plan⁵⁸ was used for training with no

major modification, apart from introducing the gaze volume as an additional input channel. 3D nnUNet models were trained on the lesion pseudo-segmentation ground truth from the GazeXPERt dataset. Gaze heatmap volumes were created from raw gaze trajectories (see “3D processed volumes” under Data Records), with each voxel counting how often gaze trajectory intersects it after flattening out the temporal dimension. Gaze from experienced and trainee readers were combined (i.e., union) for input. 5-fold cross validation experiments were performed and the average DICE score is reported.

Results: The nnUNet model incorporating expert gaze attention heatmaps performed significantly better (Table 1), despite readers spending less than 8% of their time directly viewing tumors. The majority of reading time was devoted to whole-body search for corroborating imaging findings — supporting our hypothesis that expert search patterns contain rich diagnostic information that can be distilled into AI models and collected unobtrusively from routine radiology workflow

	Dice Score	Lesion Level Metrics	
		Precision	Recall
w/o Gaze	0.601 ± 0.023	0.506 ± 0.053	0.774 ± 0.023
with Gaze	0.682 ± 0.012	0.665 ± 0.033	0.857 ± 0.035

Table 1. 3D nnUNet lesion segmentation performance with and without expert static gaze insight.

Experiment 2: Last gaze point correction to improve lesion selection in a dynamic setting. The cost of eye tracking devices can range widely (200–20,000 USD) depending on their licensing, setup, tracking rate (up to 500 Hz), accuracy and precision. We show that modeling of task-specific sequential eye tracking data can improve tracking accuracy for a more affordable and nonintrusive 60 Hz screen-based eye-tracking device when taking into account both the gaze patterns and the underlying images visualized.

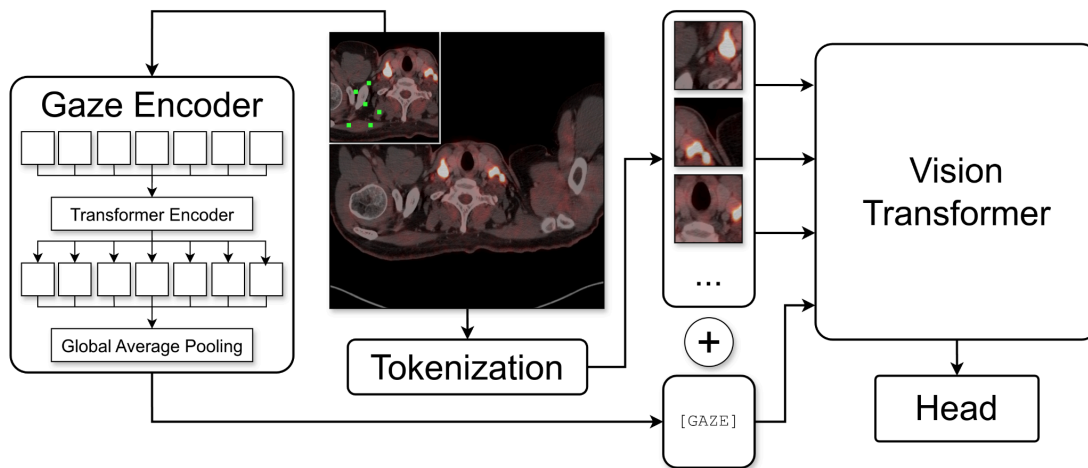


Figure 2. Transformer-based Gaze + Vision architecture. Gaze tokens derived from the

trajectory are encoded into a [GAZE] token, then processed jointly by pretrained ViT.

Method: We postprocess the GazeXPERt dataset, which initially derived 9030 accepted gaze-to-lesion tracking videos (See Data Records for COCO-style processed data). Invalid gaze samples were skipped and lesions with average gaze more than 100 pixels away were filtered, leaving $n=8610$ lesion videos (6947 train, 617 val, 1046 test) suitable for this experiment. An image-based Vision Transformer (ViT) model pretrained on ImageNet ViT/B-32 was extended by a Gaze Encoder module, and was jointly trained to predict a gaze point closer to the target lesion than the last gaze point (Figure 2). Specifically, the model inputs are up to 16 gaze coordinate samples before a lesion selection keystroke and the associated axial slice view image for the accepted lesion keystroke. We modified the ViT’s CLS token and replaced it with learned gaze information. The Gaze Encoder in Figure 2 is a normal transformer encoder, where tokenization is learned embedding and positional encoding is the same as in the original transformer paper. Loss is the average Hausdorff distance function between predicted point and all segmented pixels (as point coordinates), and is minimized when the prediction is in the center of a lesion.

	On Mask? (%)	Improved Prediction? (%)	Distance (°)
Raw Last Gaze	6.11%	-	1.134°
Predicted Gaze	18.12%	74.95%	0.856°

Table 2. Gaze correction experiment results. Average performance over 10 randomly initialized runs.

Results: For evaluation, 10 randomly seeded runs on the test split (Table 2) showed 74.95% of the predicted gaze points are closer to the target lesions than the last gaze point. The results indicate that task-specific gaze correction modeling with temporal gaze and image search pattern data is able to lower the average gaze angle error for a dynamic targeting task from 1.134° uncorrected to 0.856° post correction, which is then within the expected range (0.5°-1°) for static targeting tasks.

Experiment 3: Task-specific human expert intention prediction.

The last of our hypotheses is that temporal gaze data can be used to facilitate interaction between AI models and the human experts. Target lesion detection and measurement is a specific clinically useful goal for accelerating efficient FDG-PET/CT reads. However, readers spend the majority of the read time searching for imaging clues leading up to an intended target lesion, making the task of intention prediction non-trivial. Therefore, we trained a model to validate the feasibility of using gaze trajectory and its corresponding slice images to differentiate “intentional” targeting versus “unintentional” searching.

Method: We modeled this problem as a binary classification task. Gaze trajectories and corresponding slice images of accepted lesions are used as “intentional” samples (13126

train, 1391 val, 1906 test). Random non-tumor PET hot spots and their preceding gaze trajectory and images are used to simulate “unintentional” samples (12563 train, 1209 val, 1870 test). We used the same vision transformer model architecture (see Figure 2) and similar input compared to experiment 2, with the difference being that the gaze trajectory used is longer (minimum 1 second, maximum 2 second at 60 Hz) and continuous, and that the model is trained with focal loss.

Results: Our results show that human intention prediction or understanding via gaze is not easy or a solved problem but is trainable, at least when posed as a classification problem (Table 3). More advanced temporal modeling of sequential gaze and PET/CT images in future work will likely improve on these baseline results.

Accuracy	Balanced (Macro) Accuracy	F1-Score	ROC AUC
67.53% \pm 1.63	67.51% \pm 1.64	0.673 \pm 0.016	0.747 \pm 0.024

Table 3. Intention prediction experiment: Average performance over 10 randomly initialized runs.

Discussions

Limitations and Dataset Usage Notes

There are a few limitations in the GazeXPERt annotation methodology. First, PET/CT reading parameters were simplified to a single viewing window, whereas real-world workflows involve multiple screens and comparison of sequential studies — differences we view predominantly as software engineering challenges for future efforts.

Second, pseudosegmentation ground truth is difficult to obtain for lesions with indistinct margins, similar FDG uptake to background, or heterogeneous uptake. These complex cases constitute a small portion of GazeXPERt given the hypermetabolic cancer types included, but challenges may arise with less hypermetabolic cancers or those in high-background-uptake organs. Variability in PET/CT acquisition parameters may also introduce gaze pattern heterogeneity that should be considered when training downstream models.

Lastly, validation experiments used established gaze processing methods and AI architectures without significant modification or gaze pretraining. More sophisticated gaze processing and modeling represent key future research directions for developing interactive agents that understand expert intentions.

Summary and Future Work

We demonstrated basic gaze postprocessing techniques that render complex raw gaze data useful for baseline tasks, including 3D volumetric lesion segmentation with expert insight and multimodal temporal gaze prediction. These represent only a subset of the research problems GazeXPERt is designed to support. Additional future directions include visual grounding, causal reasoning, human intention prediction, and expert gaze-rewarded modeling.

GazeXPERt addresses a critical and underexplored gap: the scarcity of large-scale, machine learning-ready datasets that embed expert visual reasoning into the AI development pipeline. Most existing lesion detection and segmentation models treat imaging data in isolation, offering no mechanism to ground model behavior in how expert physicians actually search and interpret oncologic scans. By capturing 9,030 gaze-to-lesion trajectories across 346 FDG-PET/CT studies in a simulated routine read workflow, GazeXPERt provides the research community with a valuable resource for developing FDG-PET/CT AI models that are not only accurate, but interpretable and explainable by design — a distinction increasingly essential for clinical translation and regulatory acceptance.

The dataset's impact is expected to span several high-priority research frontiers. In interpretable AI, GazeXPERt enables models whose attention can be grounded against real expert gaze, moving beyond post-hoc saliency approximations. In gaze-rewarded

reinforcement learning, it offers human-derived reward signals to guide agents toward expert-like search strategies. In human-AI interaction, it supports adaptive systems that flag overlooked findings, prioritize regions of interest, or calibrate assistance to inferred reader intent — directly aligned with clinical priorities around efficiency, transparency, and reduced cognitive burden in high-volume oncologic imaging.

Overall, in contributing GazeXPERt, our goal is not only to advance interpretable and explainable lesion detection and segmentation models, but to catalyze a new generation of expert gaze-rewarded AI systems capable of understanding and augmenting physician reasoning in real time — bringing us closer to AI that earns, rather than assumes, the trust of the clinicians it is designed to support.

Main Text Word count: 2958

Data and Code Records

The GazeXPERt dataset will be hosted on multiple platforms, including the Stanford Center for Artificial Intelligence in Medicine and Imaging (AIMI Center) and Kaggle. [During peer review, the dataset will only be hosted at: https://stanford.redivis.com/datasets/460a-2j4r7trr](https://stanford.redivis.com/datasets/460a-2j4r7trr). Please see detailed Data Records in Supplemental Material 2 and 3. Code and detailed software version information for the gaze data postprocessing and the validation experiments is available at: <https://zivgitlab.uni-muenster.de/cvmls/gazexpert>.

Ethical Statement:

IRB waiver was obtained from Stanford Health Care to add expert eye-tracking insight and new independent lesion annotations to an existing de-identified public dataset¹⁹. The research project also obtained a data use agreement from Tübingen for usage of the FDG-PET/CT images for eye-tracking AI interpretability and explainability research.

Disclosure of AI Usage:

The authors first manually prepared the manuscript. A Large language model (LLM)-based AI tool (Anthropic Sonnet 4.6 on 02/20/2026) was used to assist with final shortening and text refinement of the abstract and discussions sections. All scientific content, data, analyses, figures, and conclusions are made by and solely the responsibility of the authors.

Acknowledgements

- Nuclear Medicine and Molecular Imaging, Department of Radiology, Stanford University/Stanford Health Care, for data collection spaces.
- Computer Vision and Machine Learning Systems, University of Münster for compute resources.
- Stanford AIMI Center for hosting the GazeXPERt dataset for open sourcing.
- Google Academic Research Credits Program for data storage and compute resources in the cloud.
- The authors thank Andrew Zhang and Suvan Chauhan for their help in an earlier phase of the project.

Competing Interests

The authors declare no competing interests. The eye-tracking platform was funded by the Stanford AIMI Center. Otherwise, there is no funding for this work.

Author contributions statement

All authors reviewed the manuscript. Specific contributions are as follow:

- Joy T Wu (*first equal) - clinical concept conception, idea development and application framing for FDG-PET/CT, building data collection platform, sourcing hardware and team, collecting data, exploratory analysis, model development, literature review, writing and editing manuscript, coordinating and driving the project.
- Daniel Beckman (*first equal) - idea development, building data collection platform, main model development and training, exploratory analyses, literature review, writing and editing manuscript.
- Sarah Miller - idea development, collecting data, coordinating project, literature review, writing and editing manuscript. • Alexander Lee - collecting data, independent data quality review, reviewing manuscript.
- Elizabeth Theng - collecting data, exploratory data analysis, literature review, editing and reviewing manuscript. • Stephan Altmayer - collecting data, editing and reviewing manuscript.
- Ken Chang - collecting data, reviewing manuscript.
- David Kersting - collecting data, reviewing manuscript.
- Tomoaki Otani - collecting data, reviewing manuscript.
- Brittany Z Dashevsky - collecting data, reviewing manuscript.
- Hye Lim Park - collecting data, reviewing manuscript.
- Matteo Novello - collecting data, reviewing manuscript.
- Kip Guja - collecting data, reviewing manuscript.
- Curtis Langlotz - supervision, editing and reviewing manuscript.
- Ismini Lourentzou - supervision, literature review, editing and reviewing manuscript.
- Daniel Gruhl- idea development, key project development supervision, editing and reviewing manuscript.
- Benjamin Risse (**Senior advisor) - idea development, main technical modeling supervisor, literature review, editing and reviewing manuscript.
- Guido A Davidzon (**Senior advisor) - clinical concept conception, idea development and application framing for FDG-PET/CT, collecting data, project coordination, main clinical supervisor, literature review, editing and reviewing manuscript.

References

1. Parihar, A. S., Dehdashti, F. & Wahl, R. L. Fdg pet/ct–based response assessment in malignancies. *Radiographics* 43, e220122 (2023).
2. Wahl, R. L., Jacene, H., Kasamon, Y. & Lodge, M. A. From recist to percist: evolving considerations for pet response criteria in solid tumors. *J. nuclear medicine* 50, 122S–150S (2009).
3. Jadvar, H. *et al.* Appropriate use criteria for 18f-fdg pet/ct in restaging and treatment response assessment of malignant disease. *J. Nucl. Medicine* 58, 2026–2037 (2017).
4. Czernin, J. Clinical applications of fdg-pet in oncology. *Acta Medica Austriaca* 29, 162–170 (2002).
5. Weber, W. A. Use of pet for monitoring cancer therapy and for predicting outcome. *J. Nucl. Medicine* 46, 983–995 (2005).
6. Lardinois, D. *et al.* Staging of non–small-cell lung cancer with integrated positron-emission tomography and computed tomography. *New Engl. J. Medicine* 348, 2500–2507 (2003).
7. Boellaard, R. *et al.* Fdg pet/ct: Eanm procedure guidelines for tumour imaging: version 2.0. *Eur. journal nuclear medicine molecular imaging* 42, 328–354 (2015).
8. Avril, N. E. & Weber, W. A. Monitoring response to treatment in patients utilizing pet. *Radiol. Clin.* 43, 189–204 (2005).
9. Fletcher, J. W. *et al.* Recommendations on the use of 18f-fdg pet in oncology. *J. Nucl. Medicine* 49, 480–508 (2008).
10. Delgado-Bolton, R. C., Fernández-Pérez, C., González-Maté, A. & Carreras, J. L. Meta-analysis of the performance of 18f-fdg pet in primary tumor detection in unknown primary tumors. *J. Nucl. Medicine* 44, 1301–1314 (2003).
11. Gregoire, V. & Chiti, A. Pet in radiotherapy planning: particularly exquisite test or pending and experimental tool? *Radiother. Oncol.* 96, 275–276 (2010).
12. Thorwarth, D. *et al.* Integration of fdg-pet/ct into external beam radiation therapy planning. *Nuklearmedizin NuclearMedicine* 51, 140–153 (2012).
13. Hofman, M. S. & Hicks, R. J. How we read oncologic fdg pet/ct. *Cancer Imaging* 16, 35 (2016).
14. Zhang, H. *et al.* Prognostic value of metabolic tumor burden from 18f-fdg pet in surgical patients with non–small-cell lung cancer. *Acad. radiology* 20, 32–40 (2013).
15. Meignan, M., Cottreau, A.-S., Specht, L. & Mikhaeel, N. G. Total tumor burden in lymphoma—an evolving strong prognostic parameter. *The Br. journal radiology* 94, 20210448 (2021).
16. Gatidis, S. *et al.* Results from the autopet challenge on fully automated lesion segmentation in oncologic pet/ct imaging. *Nat. Mach. Intell.* 6, 1396–1405 (2024).
17. Grossiord, E., Talbot, H., Passat, N., Meignan, M. & Najman, L. Automated 3d lymphoma lesion segmentation from pet/ct characteristics. In *2017 IEEE 14th international symposium on biomedical imaging (ISBI 2017)*, 174–178 (IEEE, 2017).
18. Eyuboglu, S. *et al.* Multi-task weak supervision enables anatomically-resolved abnormality detection in whole-body fdg-pet/ct. *Nat. communications* 12, 1880 (2021).

19. Gatidis, S. *et al.* A whole-body fdg-pet/ct dataset with manually annotated tumor lesions. *Sci. Data* 9, 601 (2022).
20. Xia, Q. *et al.* A comprehensive review of deep learning for medical image segmentation. *Neurocomputing* 613, 128740 (2025).
21. Salimi, Y., Mansouri, Z., Amini, M., Mainta, I. & Zaidi, H. Explainable ai for automated respiratory misalignment detection in pet/ct imaging. *Phys. Medicine & Biol.* 69, 215036 (2024).
22. Mbakwe, A. B., Lourentzou, I., Celi, L. A. & Wu, J. T. Fairness metrics for health ai: we have a long way to go. *EBioMedicine* 90 (2023).
23. Sundar, L. K. S. & Beyer, T. Is automatic tumor segmentation on whole-body 18f-fdg pet images a clinical reality? *J. Nucl. Medicine* 65, 995–997 (2024).
24. Droguet, M. *et al.* Automated segmentation of lesions in [18f] fdg pet/ct images of lung cancer patients: external evaluation of an ai-driven lesion segmentation tool (lion) (2024).
25. Froad, R. *et al.* Comparative effectiveness of standard vs. ai-assisted pet/ct reading workflow for pre-treatment lymphoma staging: a multi-institutional reader study evaluation. *Front. Nucl. Medicine* 3, 1327186 (2024).
26. Khosravan, N. *et al.* A collaborative computer aided diagnosis (c-cad) system with eye-tracking, sparse attentional model, and deep learning. *Med. image analysis* 51, 101–115 (2019).
27. Hayhoe, M. & Ballard, D. Modeling task control of eye movements. *Curr. Biol.* 24, R622–R628 (2014).
28. Foulsham, T. Eye movements and their functions in everyday tasks. *Eye* 29, 196–199 (2015).
29. Van der Gijp, A. *et al.* How visual search relates to visual diagnostic performance: a narrative systematic review of eye-tracking research in radiology. *Adv. Heal. Sci. Educ.* 22, 765–787 (2017).
30. Waite, S. *et al.* Analysis of perceptual expertise in radiology—current knowledge and a new perspective. *Front. human neuroscience* 13, 213 (2019).
31. Mall, S., Brennan, P. C. & Mello-Thoms, C. Modeling visual search behavior of breast radiologists using a deep convolution neural network. *J. medical imaging* 5, 035502–035502 (2018).
32. Karargyris, A. *et al.* Creation and validation of a chest x-ray dataset with eye-tracking and report dictation for ai development. *Sci. data* 8, 92 (2021).
33. Saab, K. *et al.* Observational supervision for medical image classification using gaze data. In *International conference on medical image computing and computer-assisted Intervention*, 603–614 (Springer, 2021).
34. Wang, S. *et al.* Improving self-supervised medical image pre-training by early alignment with human eye gaze information. *IEEE Transactions on Med. Imaging* (2025).
35. Zhou, F., Yang, X. J. & De Winter, J. C. Using eye-tracking data to predict situation awareness in real time during takeover transitions in conditionally automated driving. *IEEE transactions on intelligent transportation systems* 23, 2284–2295 (2021).
36. Cho, S.-W., Lim, Y.-H., Seo, K.-M. & Kim, J. Integration of eye-tracking and object detection in a deep learning system for quality inspection analysis. *J. Comput. Des. Eng.* 11, 158–173 (2024).

37. Zhang, Z., Crandall, D., Proulx, M., Talathi, S. & Sharma, A. Can gaze inform egocentric action recognition? In *2022 Symposium on Eye Tracking Research and Applications*, 1–7 (2022).
38. Hessels, R. S. & Hooge, I. T. Eye tracking in developmental cognitive neuroscience—the good, the bad and the ugly. *Dev. cognitive neuroscience* 40, 100710 (2019).
39. Rizzo, A., Ermini, S., Zanca, D., Bernabini, D. & Rossi, A. A machine learning approach for detecting cognitive interference based on eye-tracking data. *Front. Hum. Neurosci.* 16, 806330 (2022).
40. Duan, J., Zhang, M., Song, M., Xu, X. & Lu, H. Eye tracking-enhanced deep learning for medical image analysis: A systematic review on data efficiency, interpretability, and multimodal integration. *Bioengineering* 12, 954 (2025).
41. Moradizyev, S. *et al.* When eye-tracking meets machine learning: A systematic review on applications in medical image analysis. *arXiv preprint arXiv:2403.07834* (2024).
42. Bigolin Lanfredi, R. *et al.* Reflax, a dataset of reports and eye-tracking data for localization of abnormalities in chest x-rays. *Sci. data* 9, 350 (2022).
43. Pham, T. T. *et al.* Fg-cxr: a radiologist-aligned gaze dataset for enhancing interpretability in chest x-ray report generation. In *Proceedings of the Asian conference on computer vision*, 941–958 (2024).
44. Ma, C. *et al.* Eye-gaze guided multi-modal alignment for medical representation learning. *Adv. Neural Inf. Process. Syst.* 37, 6126–6153 (2024).
45. Wang, B. *et al.* Gazegnn: A gaze-guided graph neural network for chest x-ray classification. In *Proceedings of the IEEE/CVF Winter Conference on Applications of Computer Vision*, 2194–2203 (2024).
46. Zhu, H., Salcudean, S. & Rohling, R. Gaze-guided class activation mapping: Leverage human visual attention for network attention in chest x-rays classification. In *Proceedings of the 15th International Symposium on Visual Information Communication and Interaction*, 1–8 (2022).
47. Khaertdinova, L., Pershin, I., Shmykova, T. & Ibragimov, B. Gaze-assisted medical image segmentation. *arXiv preprint arXiv:2410.17920* (2024).
48. Stember, J. N. *et al.* Eye tracking for deep learning segmentation using convolutional neural networks. *J. digital imaging* 32, 597–604 (2019).
49. Khosravan, N. *et al.* Gaze2segment: a pilot study for integrating eye-tracking technology into medical image segmentation. In *Bayesian and graphical Models for Biomedical Imaging*, 94–104 (Springer, 2016).
50. Pham, T. T. *et al.* Ct-scangaze: A dataset and baselines for 3d volumetric scanpath modeling. In *Proceedings of the IEEE/CVF International Conference on Computer Vision*, 21732–21743 (2025).
51. Rostianingsih, S., Setiawan, A. & Halim, C. I. Coco (creating common object in context) dataset for chemistry apparatus. *Procedia Comput. Sci.* 171, 2445–2452 (2020).
52. Tobii Pro. Spark eye tracker (Pro Spark). Apparatus and software (2019).
53. Hooge, I. T. *et al.* Eye tracker calibration: How well can humans refixate a target? *Behav. Res.*

Methods 57, 23 (2024).

54. Jacene, H. A. *et al.* Assessment of interobserver reproducibility in quantitative 18f-fdg pet and ct measurements of tumor response to therapy. *J. Nucl. Medicine* 50, 1760–1769 (2009).
55. Constantino, C. S. *et al.* Evaluation of semiautomatic and deep learning–based fully automatic segmentation methods on [18f] fdg pet/ct images from patients with lymphoma: influence on tumor characterization. *J. Digit. Imaging* 36, 1864–1876 (2023).
56. Kudura, K. *et al.* Malignancy rate of indeterminate findings on fdg-pet/ct in cutaneous melanoma patients. *Diagnostics* 11, 883 (2021).
57. Moses, W. W. Fundamental limits of spatial resolution in pet. *Nucl. Instruments Methods Phys. Res. Sect. A: Accel. Spectrometers, Detect. Assoc. Equip.* 648, S236–S240 (2011).
58. Isensee, Fabian, *et al.* nnU-Net: a self-configuring method for deep learning-based biomedical image segmentation. *Nature methods* 18.2 (2021): 203-211.

Supplemental Appendix 1:

Eye-Tracking and Lesion Detection Data Collection Protocol

Goal: Create a dataset of gaze patterns for detecting FDG-avid tumors on [18F] FDG-PET/CTs.

Clinical tasks:

1. Read FDG-PET/CTs to spot, correct if needed, and confirm metabolically active tumor lesions. No report generation is required.
2. Indicate whether you are 'certain' or 'uncertain' that an FDG-avid lesion is caused by a tumor. 'Uncertain' hypermetabolic foci are findings that you would want to mention in a report for attention on follow up, which includes any focal FDG uptake that you think may be due to cancer but may also have another physiological explanation (e.g. reactive lymph node, skin thickening near cancer surgical sites, etc).
3. Use radiology "search patterns" that you would normally use for 1) and 2).

Objectives and Background:

- Enable gaze as an additional input to aid with more efficient and reproducible radiology reads, starting with lesion detection and measurement on FDG-PET/CTs.
- Build A.I. models that can understand and anticipate radiologists' intentions via their gaze and interactively assist them in their workflow with as little interruption as possible.
- The work aims to address challenges in A.I. interpretability, explainability, trust, robustness, and ease of model adoption in real-life workflows.

Setting Expectations:

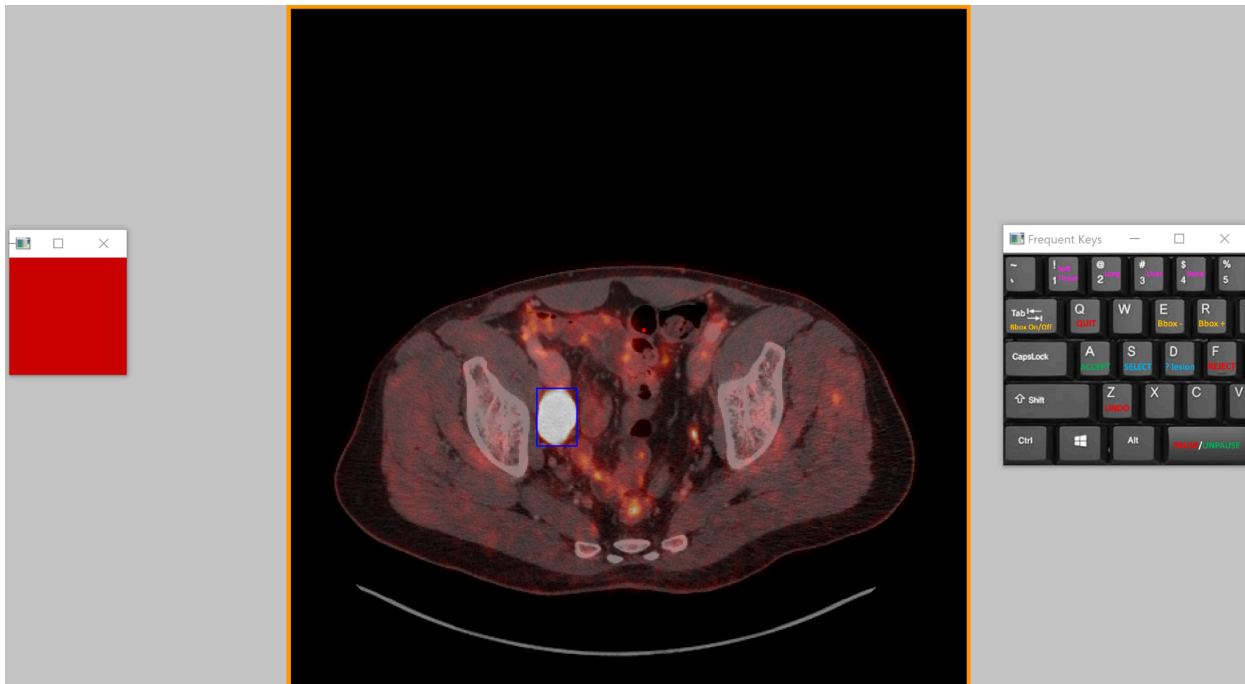
- **You're NOT required to generate a clinical report to read a PET/CT study.**
- A specially developed eye-tracking platform/viewer will collect your gaze patterns (x, y coordinates) without collecting any identifying information (e.g., face).
- You will be able to read the PET/CT study in 1 single window in axial and MIP views.
- The data collection UI will propose tumor candidates based on your gaze and the images you viewed. You will need to 'accept', correct (resize), or 'reject' the proposed tumor candidate.
- The collected gaze annotation data will be published in an open source dataset.
- Most PET/CT studies have 5-20 lesions. Less than 10 in the whole PET/CT dataset have up to 50 lesions. Collections of 15 studies will be randomly sampled and assigned.
- Most studies take 3-5 minutes to finish reading.
- Contribution-based co-authorship: you must help with paper review and writing, and optionally data processing or modeling, according to your skills and interests.

Eye Tracking UI Functionality and Keys:

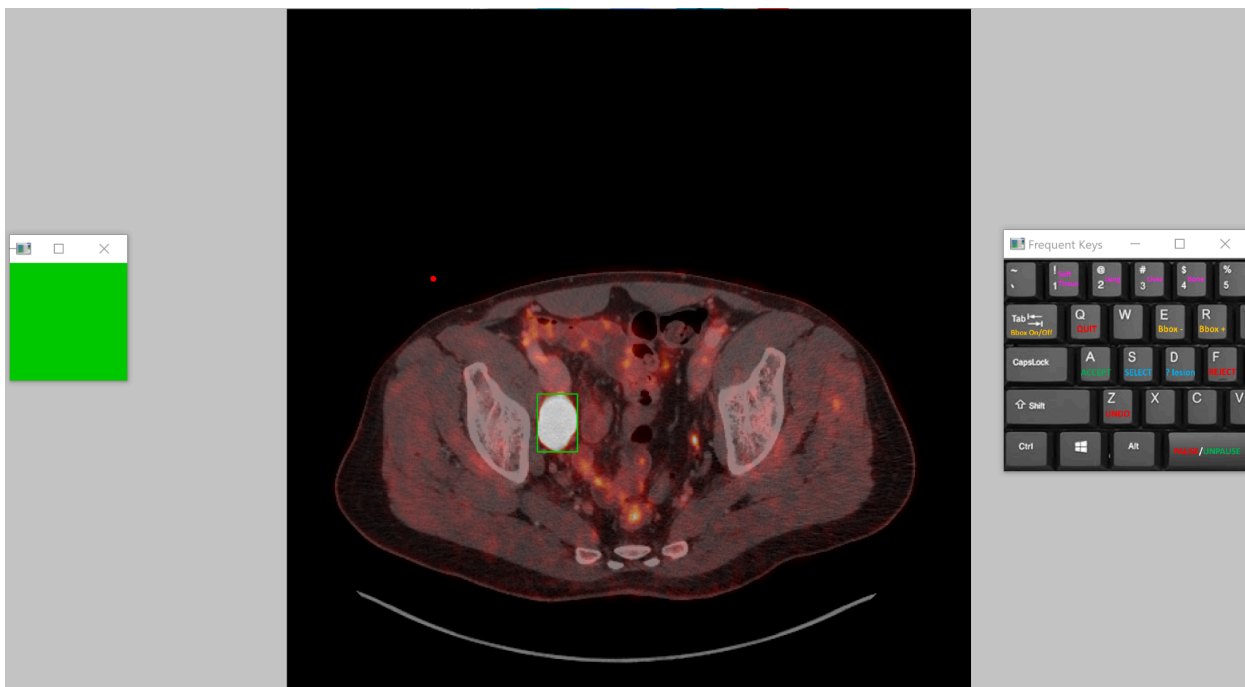
Key/Mouse	Functionality
'Spacebar'	Pause (red top left box) or unpause (start, Green top left box) gaze recording.
'q'	Quit/close the eye-tracking User Interface (UI).
'y' + 'Enter'	Yes, save the gaze recording for the PET/CT read.
'n' + 'Enter'	No, do not save the current gaze recording as you plan to repeat later.
'p'	Show PET modality image only.
'c'	Show CT modality image only.
'o'	Show fused (overlay) PET/CT modality images.
'm'	Show MIP projection of the PET images.
'l'	Show PET or PET/CT with liver contrast level (SUV max ~ 5-6)
'b'	Show PET or PET/CT with brain contrast level (SUV max > 20)
'+' or right mouse click	Increase PET contrast. (No need to press 'Shift')
'-' or left mouse click	Decrease PET contrast. (No need to press 'Shift')
'>' or scroll	Go to the next image slice. (No need to press 'Shift')
'<' or scroll	Go to the previous image slice. (No need to press 'Shift')
's'	'Select' a hypermetabolic lesion you are 'certain' to be a tumor/met.
'd'	Select a hypermetabolic lesion that you are 'uncertain' to be a tumor/met.
'a'	'Accept' the selected candidate lesion (on all adjacent related slices).
'f'	Reject the selected 'false' candidate lesion on the current slice. 'Shift' then 'f' (outside the confirmation mode) rejects the lesion on all adjacent slices.
'r'	Increase the size of the candidate lesion bounding box.
'e'	Decrease the size of the candidate bounding box.
'Tab'	Turn the bounding box annotation display on or off. Won't delete anything.
'1' to '9'	Show the same CT windowing as what you are used to with Sectra.
'z'	Undo a prior accepted lesion on the current and across all its adjacent slices.

The eye tracking UI shows some of the frequently used keys in the **Frequent Keys** window on the right. These keys can be operated by just your left hand. Your keyboard is also labeled.

The UI below is in lesion **confirmation** (accept or reject) **mode**. The **candidate lesion** is bounded by a **blue** bounding box. The **PET/CT window** is bordered in **orange**. The **Recording Status** window (left) is in **red**, indicating your gaze is currently not being recorded (i.e. paused).

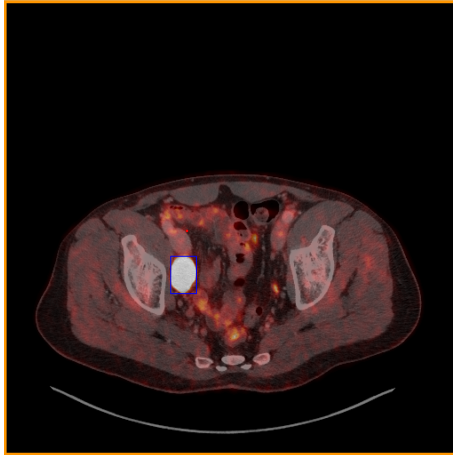


Once the candidate lesion is accepted (**green**) or rejected (**red**), the **Recording Status** window will become **green** again, indicating that your gaze recording has resumed (i.e. unpaused).

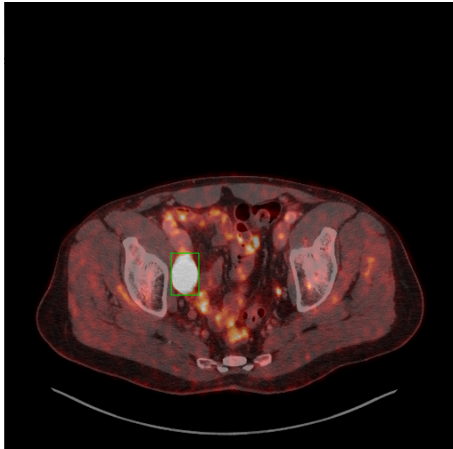


Q&A:

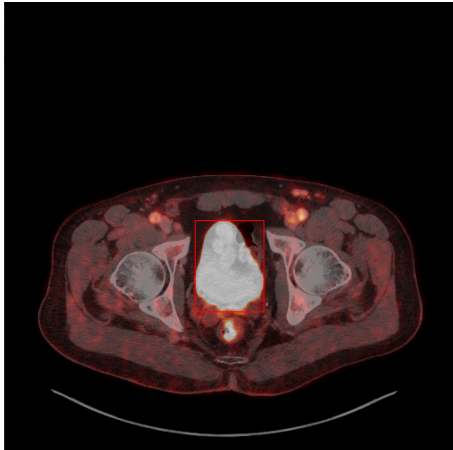
- What does a proposed 'candidate' lesion look like?
 - Will be displayed as a 'blue' bounding box. The yellow border indicates the program is waiting for the candidate lesion to be 'accepted' or 'rejected'.



-
- What does an 'accepted' lesion look like?
 - Will be displayed as a 'green' bounding box:

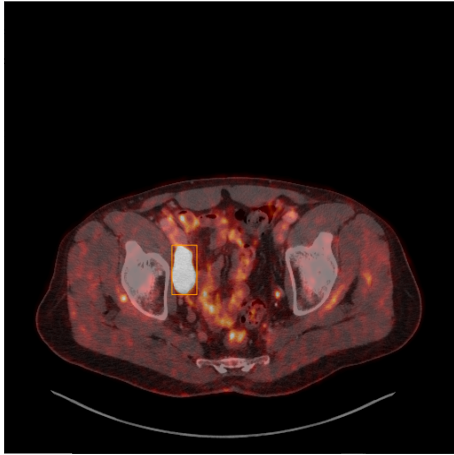


-
- What does a 'rejected' lesion look like?
 - Will stay as a 'red' bounding box. But can always go back to 'accept' it.



-
- What does an 'orange' bounding box for a lesion mean?

- Adjacent slices of the same tumor will be automatically proposed as 'orange' bounding boxes.
- **If very incorrect, please reject them, or adjust the box sizes and then accept them.**
- If correct, you could accept them or just leave/ignore them.



-
- What to do if the wrong tumor candidate is proposed when I try to select a lesion?
 - Reject the wrong candidate with the key 'f'.
 - The wrong candidate's bounding box will remain red.
 - Try selecting the correct lesion again by looking at it and pressing the key 's'.
 - Repeat the above until the correct lesion is proposed.
- What to do if no bounding box tumor candidates show up when I want to select a small mildly SUV-avid lesion?
 - You can 'right click' to increase the PET contrast to make it more conspicuous, and try selecting the now hotter appearing lesion again with the key 's'.
 - You can repeat the 'right click' and the key 's' until a bounding box lesion candidate is proposed.

Supplemental Appendix 2: Validation of Eye-Tracking Data Quality

To technically evaluate GazeXPERt’s eye-tracking data quality, we provide both gaze calibration error and inter-reader agreement analyses, and compare our results with the respective existing literature.

Gaze Calibration

As described in the methods section, each observer calibrated the eyetracker before reading using Tobii’s supplied proprietary software, which does not report calibration metrics. In addition, since the annotation task involves the observers “gaze-selecting” moving targets (lesions) while they scroll through the PET/CT image slices, we measure the task-specific gaze calibration quality using the same inter-observer study read by all observers. If an observer read the inter-observer study multiple times, the last practice run was used for this analysis. In contrast to the normal calibration procedure, which utilizes fixed point-like targets, we calculated the calibration metrics on real-world targets, i.e. on annotated lesions in the inter-observer study. Specifically, upon selecting a lesion in the annotation software, we use the gaze samples of the last 0.25 seconds leading up to the lesion selection to calculate gaze accuracy and precision. We define the center of the resultant lesion bounding box on the current (root) slice as the target point.

Gaze accuracy is defined as the mean deviation of the gaze samples from the target point, and precision is calculated as the root mean square (RMS) between consecutive gaze samples. We report both metrics in terms of degrees angle between the two gaze vectors from the eye position (i.e., the gaze origin) to the recorded gaze sample and the target point, respectively. Across all observers (total N=149 with average 11.4 lesion calibration points per observer), we report a mean accuracy of 1.176° with a standard deviation of 0.692, and a precision of 0.314° with a standard deviation of 0.167. Table 4 shows in detail the distance of the last and closest gaze points within the last 0.25 seconds to the target, respectively:

In comparison to static calibration numbers in the literature, our dynamic precision is within the expected range of 0.1° to 0.5° , while accuracy lies below the usually reported range of 0.3° to 0.75° for static tasks⁵³. The lower accuracy may in part be attributed to the nature of our task, which involves selecting dynamic moving targets, as lesions pop in and out of field of view on axial images. i.e. observers are not expected to look directly at the center of the lesion when using our eye-tracking enabled PET/CT annotation software.

	Mean (std)	Median	Min	Max
Last Gaze Point	1.068 ± 0.672	0.754	0.483	3.056
Closest Gaze Point	0.837 ± 0.648	0.604	0.269	2.811

Table 4. Distance of the last and closest gaze points from the lesion centers, across all participants and lesions.

Inter-Annotator Agreement

In order to further assess the annotation quality of the GazeXPERt dataset, we compare our two independent overreads to each other and to the original "Tubingen" annotation provided by Gatidis et al¹⁹. The analyses do not intend to imply which set of ground truth is "more correct" since the annotation tasks and goals between Tubingen and the GazeXPERt dataset are inherently different, and the two datasets are intended to be used synergistically. We analyzed the agreement between the three different sets of lesion annotations at the 3D lesions level. Since our annotation method yields bounding boxes, we transform the segmentation ground truth from the Tubingen dataset accordingly.

We calculated the standard average fixed raters Intraclass Correlation Coefficient (ICC) metric (via Python package Pinguoin version 0.5.5), which is the metric used in the FDG-PET/CT segmentation inter-reader comparison literature^{54, 55}. However, since ICC only accounts for matching lesions, we also calculate additional precision, recall and percentage inter-observer agreement ($\frac{TP}{TP + FP + FN}$) metrics between the three sets of annotations. For the latter analysis, due to predominantly small lesions (objects) in the dataset, a match (TP) is calculated at Intersection over Union (IoU) greater than 0.

Table 5 summarizes our findings. Overall, the inter-reader agreement by ICC metrics across all 3 sets of annotations fall within the reported ICC range (0.4-0.9) in the existing literature for FDG-PET/CT lesion measurement^{54, 55}. Of the matching lesions, GazeXPERt trainees and experienced annotations do agree more with each other than with the Tubingen the annotations by Gatidis et al¹⁹, which is expected given their shared task instruction, setup and overall practice environment. Across all lesion annotations, the GazeXPERt experienced readers do agree more with the Tubingen annotations than trainees, although the difference is not statistically significant at the 95% confidence interval. The trainees also have more overcalled lesions relative to both the GazeXPERt and Tubingen annotations, predominantly due to small uncertain lesions.

	Precision	Recall	% Agreement	ICC [95% CI]
Trainee ↔ Experienced	0.8130	0.8165	0.6748	0.76 [0.75-0.78]
Trainee ↔ Tubingen	0.8355	0.8371	0.7140	0.70 [0.68-0.73]
Experienced ↔ Tubingen	0.8560	0.8668	0.7600	0.74 [0.72-0.76]
GazeXPERt Union ↔ Tubingen	0.8458	0.8519	0.7369	0.73 [0.71-0.75]

Table 5. Three Way Inter-reader Lesion Annotation Agreement Analysis between GazeXPERt and Tubingen dataset.

Figure 3 breaks down and visualizes the inter-reader agreement between the three sets of annotations by lesion sizes. Almost all disagreed lesions are small, with the majority smaller than 1 cm, which tend to be the most likely to be clinically indeterminate in routine practice,

from a combination of co-existence of multiple reasonable differential diagnoses and physical limits of PET resolution (6-8 mm)^{56, 57}. In oncologic FDG-PET/CT, such findings frequently do not alter immediate management and are often followed longitudinally rather than definitely classified at a single time point. Therefore, reduced agreement in this subset reflects realistic diagnostic ambiguity rather than annotation error and highlights the importance of incorporating uncertainty into downstream modeling. The GazeXPET lesion annotation also included an “uncertain” versus “certain” tag for all accepted tumor lesions to account for this uncertainty in future model training.

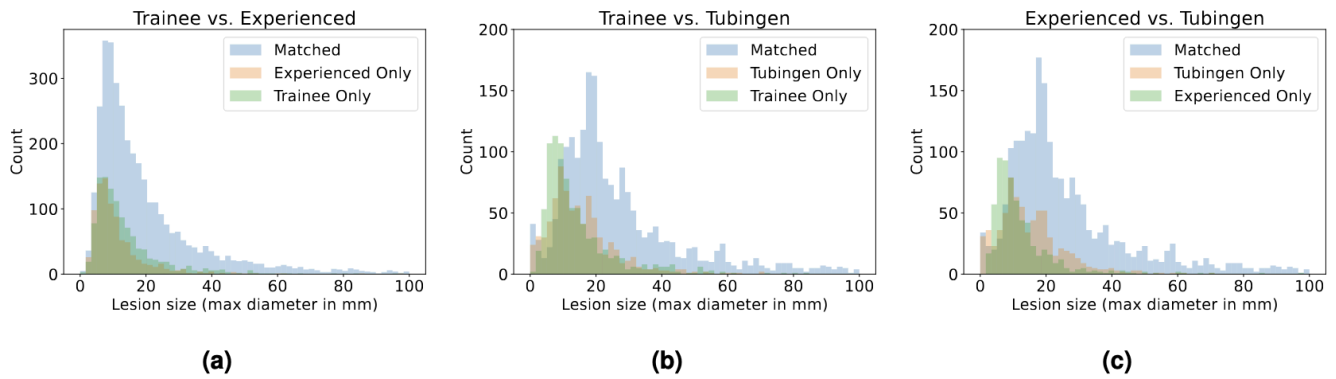


Figure 3. Inter-Reader Agreement across lesion sizes between GazeXPET and Tubingen lesions.

In clinical FDG-PET/CT interpretation, lesion detection is inherently context and decision-driven rather than purely exhaustive. Expert readers prioritize FDG-avid lesions differently depending on the clinical context, such as baseline staging versus treatment response assessment, identification of index lesions, and estimation of total tumor burden. This process involves balancing sensitivity for malignant disease against avoidance of false positives arising from physiologic uptake, inflammatory changes, and therapy-related effects. As a result, visual search patterns reflect not only lesion conspicuity but also higher-order clinical reasoning that evolves dynamically during interpretation. In routine interpretations, experts often implicitly prioritize so-called "index lesions" that are most representative of disease activity or most likely to influence management, while de-emphasizing small or clinically inconsequential findings. Such prioritization is reflected in gaze dwell time, revisit frequency, and interaction patterns. The GazeXPET dataset aims to naturally capture this reasoning process to teach AI models.

Supplemental Appendix 3: Data Records

Dataset Structure Overview

The GazeXPERt dataset consists of two sets of added expert visual insight (gaze trajectories) and lesion-level annotations in the form of raw JSONs and post-processed gaze segmentation volumes indexed to the source dataset. The original PET/CT images came from the open-source Tubingen dataset, and both datasets are shared under the Creative Commons Attribution 4.0 International License (CC BY 4.0). The highest level structure of the GazeXPERt repository is organized as in Figure 4, where the highlighted "FDG-PET-CT-Lesions" folder will need to be separately downloaded from Tubingen (see setup instructions from our GitHub repository).

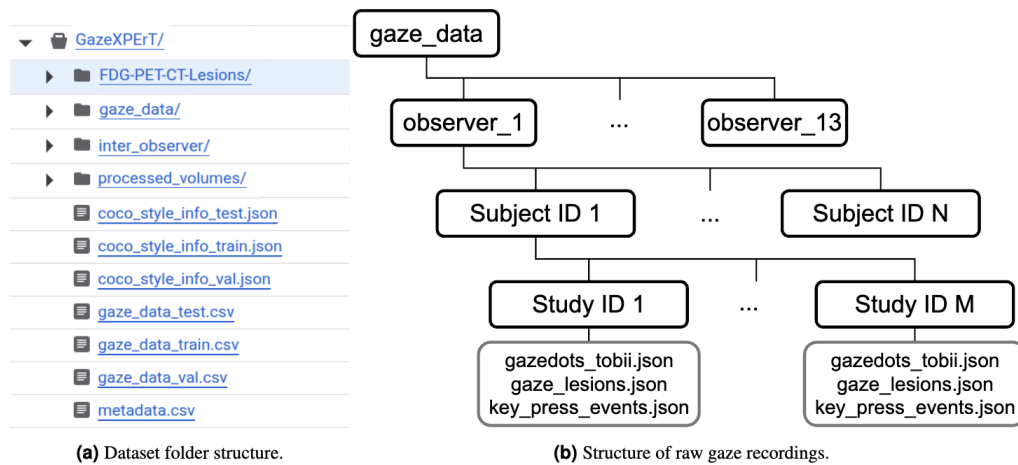


Figure 4. GazeXPERt dataset structure overview. Figure 4a depicts the top-level folder structure, Figure 4b illustrates the structure of raw recordings, following the Tubingen dataset structure.

The "gaze_data" folder contains the raw eye-tracking data in the GazeXPERt dataset. The "inter-observer" folder contains at least 1 practice recording for each observer, which is also used for deriving gaze calibration measurement data. The "processed_volumes" folder contains the eye-tracking data rendered in 3D heatmap volume, useful for 3D modeling. The root "GazeXPERt" folder also contains the "metadata.csv", which retains the information to link recorded gaze and annotations to their respective original anonymized studies by study paths.

As shown in Figure 4b, the structures for both the "gaze_data" and the "inter_observer" folders are first organized by anonymized observer IDs, then by the original nested study paths. Each study recording folder contains three separate files for raw gaze data ("gazedots_tobii.json"), lesion annotations ("gaze_lesions.json") and key presses ("key_press_events.json") respectively. The observer ID level is removed from the structure of the "processed_volumes" folder.

Raw Gaze Data JSONs Explained

For each study read, there are three types of raw JSON files, detailed below. Code to process and utilize all the gaze JSON and CSV information is provided in our GitHub.

1) "gazedots_tobii.json" explanation (Figure 5):

- Each file contains the raw gaze and image metadata recording for the entire study read from one observe
- The fields "tobii_cam", "common_cam" and "pauses" contain elements synced by position in ordered lists.
- The "tracker_sample" shows the raw tobii data saved for each gaze point. For more information, please see user support for Tobii Pro Spark tracker.
- The "display_sample" shows the corresponding imaging metadata saved with each gaze point (at 60Hz too) to reconstruct the image in the way that the experts deemed best to visualize the PET/CT data at that point in time.
- The "pause" tag shows when the reader decided to take a break from reading, which is uncommon besides near the start and end of each read. It is also by default set to "True" in the time between a lesion "select" and its "accept" or "reject" decision key presses to tag the gaze within this time window, as there can be a small computational lag to propagate the lesion candidate bounding box annotations to image slices adjacent to the root image slice.

gazedots_tobii.json		tracker_sample	
tobii_cam: [tracker_sample, ...]		device_time_stamp: int	system_time_stamp: int
common_cam: [display_sample, ...]		left_gaze_point_on_display_area: [float, float]	
pauses: [bool, bool, bool, ...]		left_gaze_point_in_user_coordinate_system: [float, float]	
monitor_width: int	monitor_height: int	left_gaze_point_validity: int	
display_window_dim: [int, int]		left_pupil_diameter: float	
case_difficulty: int		left_pupil_validity: int	
ui_experience: int		left_gaze_origin_in_user_coordinate_system: [float, float]	
comment: str		left_gaze_origin_in_trackbox_coordinate_system: [float, float]	
display sample		right_gaze_point_on_display_area: [float, float]	
slice_number: int	modality: str	right_gaze_point_in_user_coordinate_system: [float, float]	
norm_min: float	norm_max: float	right_gaze_point_validity: int	
window_x: int	window_y: int	right_pupil_diameter: float	
window_width: int	window_height: int	right_pupil_validity: int	
monitor_width: int	monitor_height: int	right_gaze_origin_in_user_coordinate_system: [float, float]	
ct_window: int		right_gaze_origin_in_trackbox_coordinate_system: [float, float]	

Figure 5. Content overview for "gazedots_tobii.json".

2) "gaze_lesions.json" explanation (Figure 6a):

- Each file contains the subset of raw gaze recording associated with the "root" lesion annotations at the bounding box (Bbox) level. The Bboxes are stored in the "xywh" format in pixel coordinates using the display size during annotation (e.g., if displayed at 1400px, then the coordinates would be upscaled to 1400 px from the original PET/CT images' 512 px resolution).
- Each lesion annotation contains: the raw gaze coordinate at the point of lesion selection, the root accepted Bbox candidate coordinates, the candidate acceptance key used ("certain" versus "uncertain"), the corresponding image screen display parameters, all the Bboxes from all adjacent slices associated with the root lesion slice, and the PET "threshold" used to create them.
- "certainty": The observer can use two different acceptance keys to indicate how confident they are that the lesion is due to a tumor ("certain") versus another possible explanation but cannot exclude cancer ("uncertain" for e.g., metastatic versus reactive lymph node).
- "status": Whether the lesion bounding box on a slice was manually validated versus extrapolated candidates from a root-validated/accepted lesion.

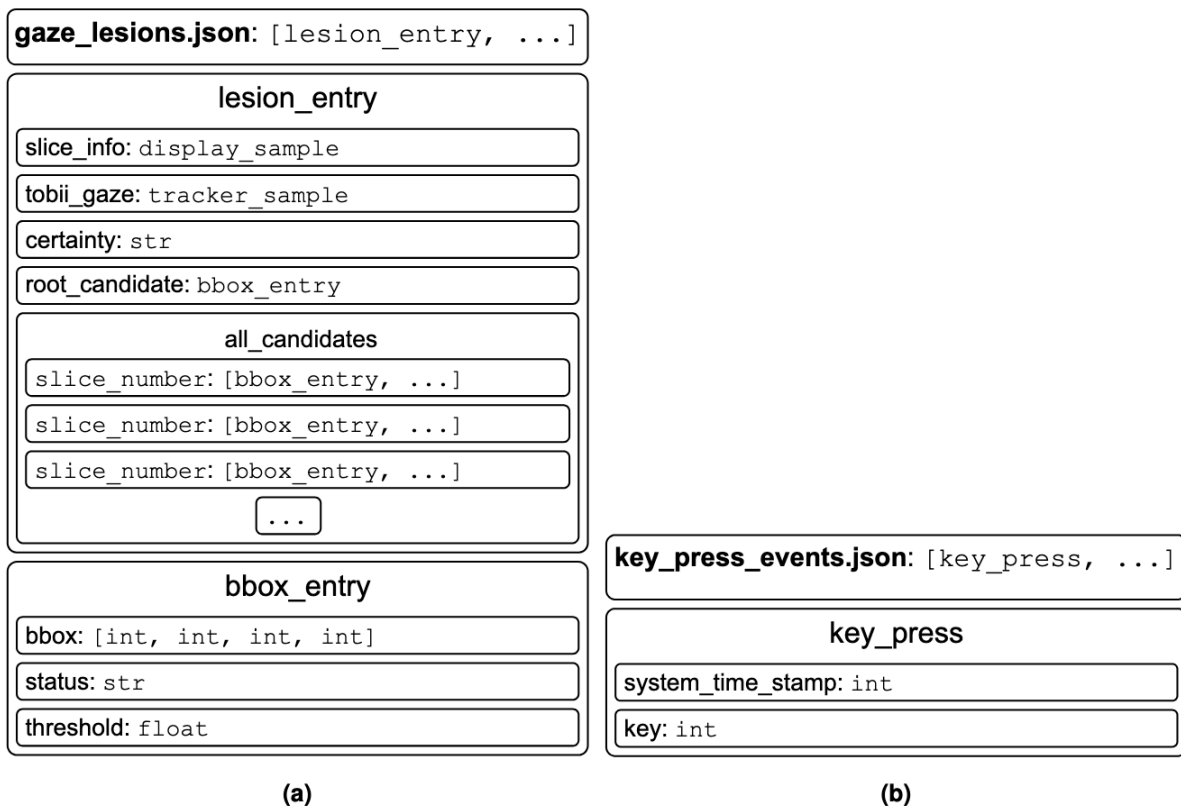


Figure 6. Content overview for "gaze_lesions.json" (a) and "key_press_events.json" (b) files, respectively. These files contain information regarding annotated lesions and all keystrokes during the annotation process.

3) “key_press_events.json” explanation (Figure 6b)

- This file allows for complete reconstruction of all the manual decisions made during the whole annotation process, including corrections, redactions, etc.
- The system timestamps sync key press events with the gaze data. All key press events (i.e., experts’ decisions) used by the observer for a study read are saved as integers recorded by the OpenCv Python library.
- Scrolling through the volume using the mouse wheel is not recorded in this file, but can be reconstructed from image slice information in the “display_samples” field from “gaze_lesions.json”.

Post-processed Gaze Data for Ease of Machine Learning Tasks

To facilitate ease of using this rich but complex medical imaging eye-tracking dataset, we have postprocessed the gaze data to 1) 3D gaze volume NIFTI files and to a 2) Common Objects in Context (COCO) style format JSONs and CSVs for different types of machine learning tasks.

1) 3D “processed volumes” NIFTI files for ease of 3D lesion segmentation-related experiments. These are kept in the “processed_volumes” folder under their relevant study paths, where * in the filenames below are replaced with either “trainee” or “experienced”.

- Processing for the 3D Gaze heatmap volume (“GAZE_*.nii.gz”) and MIP (“GAZE_MIP_*.nii.gz”) NIFTI files: Raw gaze trajectory was transformed into 3D volume with the same image shape as the original 512×512 CT study. Each voxel counts the number of gaze samples on it. The temporal component is flattened and no blurring of the aggregate data was used to keep the information “raw”. Maximal Intensity Projection (MIP) of 12 different angles of the 3D gaze heatmap volume is also generated for whole-body static analysis.
- Processing for the pseudo segmentation volume NIFTI files (“PSEUDO_SEG_*.nii.gz”): 3D segmentation labeled mask derived using the recorded SUV max threshold from the Bbox lesion annotation.

2) COCO-style format JSON and CSV files, for ease of lesion-level modeling tasks, are kept at the first level immediately below the root “GazeXPErT” folder.

- These files organize access to lesion data in the GazeXPErT dataset in a COCO-style format for machine learning experiments. There are 3 JSON (“coco_style_info_*.json”) and 3 CSV (“gaze_data_*.csv”) files, organizing annotations along the “train”, validation (“val”), and “test” splits (80/10/10) used in our validation experiments.
- These processed gaze data JSON and CSV files can be used along with the original

PET/CT images to reconstruct 9030 accepted and 2658 rejected gaze-to-lesion mini-videos.

- In addition, the COCO-style JSONs allow GazeXPET annotations to be accessible on three levels of detail. Study-read level links the annotator (observer) and raw gaze data files to the PET/CT image data. Lesion-level (i.e. object-level) aggregates the gaze data to unique lesion levels, and links individual index lesions to relevant temporal gaze data in the separate train, val, or test CSV file. Slice-Level allows each lesion Bbox to be indexed to and retrieved separately.
- • Gaze postprocessing for the CSV files: The "gaze_data_*.csv" files contain the extra temporal eye-tracking data dimension that does not fit within the standard COCO style JSON format. Again, the gaze data across studies are aggregated into one csv per train, val, test split, same as for the COCO-style format JSONs. Raw gaze from Tobii tracker is filtered to exclude invalid samples (viewing outside the annotation window or flagged invalid by Tobii). Each row in the CSV maintains the link to the source FDG-PET/CT study and the slice image, and stores the timestamps, the corresponding gaze coordinates (in 512 pixel space), and any associated lesion Bbox coordinates. The Bbox coordinates are rescaled, standardized to fit the original 512px axial PET/CT images, and saved in separate columns.